

---

---

ORDER, DISORDER, AND PHASE TRANSITION  
IN CONDENSED SYSTEM

---

---

# Semiconductor–Metal Transition in Magnetic Semiconductor Compounds at High Pressure

R. K. Arslanov<sup>†</sup>, T. R. Arslanov<sup>a,\*</sup>, I. V. Fedorchenko<sup>b</sup>, and A. L. Zheludkevich<sup>c</sup>

<sup>a</sup> Amirkhanov Institute of Physics, Dagestan Scientific Center, Russian Academy of Sciences, Makhachkala, 367003 Russia

<sup>b</sup> Kurnakov Institute of General and Inorganic Chemistry, Russian Academy of Sciences, Moscow, 119991 Russia

<sup>c</sup> Scientific and Production Center for Materials Science, National Academy of Sciences of Belarus, Minsk, 220072 Belarus

\*e-mail: arslanovt@gmail.com

Received March 23, 2019; revised June 4, 2019; accepted June 24, 2019

**Abstract**—The magnetic, transport, and magnetotransport properties of ferromagnetic  $\text{Zn}_{0.1}\text{Cd}_{0.9}\text{GeAs}_2 + 10\%$  MnAs and  $\text{Zn}_{0.1}\text{Cd}_{0.9}\text{GeAs}_2 + 15\%$  MnAs nanocomposites with a Curie temperature  $T_C \approx 310\text{--}312$  K are studied at a high pressure up to 7 GPa and room temperature. The behavior of the magnetic and electronic properties under pressure points to a magnetic transformation and a semiconductor–metal transition, which occur at the same pressure ( $P \approx 3.5$  GPa). Both compositions exhibit pressure-induced magnetoresistance in the magnetic field range up to  $H = 5$  kOe. As follows from an analysis of the experimental data, the magnetoresistance in the semiconductor–metal transition area is described by a standard  $p$ – $d$  model, which takes into account the interaction of carrier spins and the magnetic moment localized at Mn impurities. A giant magnetoresistance is detected in this region: it is maximal in comparison with the magnetoresistance at atmospheric pressure ( $\Delta\rho_{xx}/\rho_0 < 1\%$ ) for the composition with 15% MnAs clusters. The appearance of enhanced magnetoresistance and the magnetic and electronic phase transformations are mainly caused by pressure-induced changes in the matrix.

DOI: 10.1134/S106377611912001X

## 1. INTRODUCTION

The electrical resistances of most semiconductors and metallic compounds are known to change in an applied magnetic field. This phenomenon is known as magnetoresistance (MR), the principle of which is the basis of modern magnetic sensors, including the transducers of reading information in hard disks. Depending on the sign of MR, the effect can be both positive and negative, and its relative change in magnetic materials is significantly higher than in that for non-magnetic compounds. In recent years, the prospects of studying well-pronounced magnetoresistance properties (giant MR, tunneling MR, etc.) are related to so-called hybrid structures, where metallic magnetic inclusions (nanoclusters) are embedded in a nonmagnetic semiconductor matrix [1]. Since such structures have free charge carriers, the electron transport caused by their interaction with nanoclusters has a spin-dependent character [2].

It should be noted that the following factors are important among the fundamental contributions to MR: weak localization, electron–electron interaction, spin and superconducting fluctuations, and magnetic impurities [3]. In most cases, the appearance of low-

temperature negative MR in magnetic semiconductors is related to weak localization induced by the dephasing of coherent backscattering [4]. Nevertheless, negative MR, which is predominant in magnetic structures, is not always caused by weak localization, especially at the non-low temperatures at which magnetic impurities or nanoclusters play a key role in a scattering mechanism.

The appearing exchange interaction between carriers and the local magnetic moments of impurity atoms leads to a strong coupling between band and localized states, which is accompanied by a giant positive or negative MR. The negative MR considered in terms of the spin disordering theory implies that the suppression of the thermodynamic fluctuations of local magnetization in a magnetic field decreases scattering [5]. It should be noted that the impurity level induced by 3D impurities can substantially perturb the density of states at the Fermi level. For example, spin splitting under the  $p$ – $d$  hybridization of a valence band leads to the formation of two (major spin and minor spin) subbands, which are characterized by different conductivities and mobilities [6]. An increase in the scattering of spin-dependent carriers due to a change in the local potential induced by the Zeeman effect can bring about positive MR.

---

<sup>†</sup> Deceased.

The spin-dependent character of MR in diluted magnetic semiconductors [7, 8], granulated structures [9, 10], and multilayers [11] is a subject of extensive investigations, which are also performed at high pressures. The main idea is that an applied pressure should decrease MR because of a decrease in the exchange interaction. However, the opposite effect is observed in some magnetic compounds: it is explained by the pressure-induced enhancement of the exchange interaction even in the paramagnetic region [7, 12]. Therefore, the negative MR appearing at a high pressure is thought to be related to spin-dependent scattering by magnetic impurities. On the hand, the behavior of MR during pressure-induced phase transformations (electronic, structural, magnetic) is poorly understood. As was shown in [8], the behavior of phase-segregated MnAs clusters in the matrix of a II–IV–V<sub>2</sub> semiconductor has a nontrivial field dependence during the transition from the initial chalcopyrite structure to a disordered ZnS-type cubic structure.

The purpose of this work is to study the magnetic, electronic, and magnetotransport properties of Zn<sub>0.1</sub>Cd<sub>0.9</sub>GeAs<sub>2</sub> + MnAs nanocomposite hybrids in the vicinity of the semiconductor–metal transition at a high pressure. These materials are characterized by the presence of both negative and positive MR, the behavior of which is closely related to pressure-induced structural, magnetic, and electronic transitions.

## 2. EXPERIMENTAL

We measured polycrystals Zn<sub>0.1</sub>Cd<sub>0.9</sub>GeAs<sub>2</sub> + 10% MnAs and Zn<sub>0.1</sub>Cd<sub>0.9</sub>GeAs<sub>2</sub> + 15% MnAs in a high-pressure toroid apparatus at a hydrodynamics pressure  $P \leq 7$  GPa at room temperature during an increase and decrease in pressure. Pressure was generated at a constant rate of 1 GPa/h during compression. During decompression, the rate of decreasing the pressure corresponded to the rate of natural relaxation of the system, which was comparable with the direct run, and the rate of decrease was about 0.2 GPa/h below 1 GPa. The apparatus was placed in a solenoid with a field  $H \leq 5$  kOe. As a working cell, we used a 80-mm<sup>3</sup> fluoroplastic capsule with eight current leads, which allowed us to measure electrical resistivity  $\rho$ , Hall coefficient  $R_H$ , and transverse MR  $\Delta\rho_{xx}/\rho_0$  ( $\rho_0$  is the electrical resistivity in the absence of magnetic field) under pressure simultaneously. The pressure was controlled using a manganin manometer graduated against a few reference points of Bi over the entire pressure range. The experimental techniques were described in detail in [13] and the synthesis of samples and their growth conditions were described in [14].

The samples used for measuring transport and magnetotransport parameters  $\rho$ ,  $R_H$ , and  $\Delta\rho_{xx}/\rho_0$  by a six-probe method were  $3 \times 1 \times 1$ -mm<sup>3</sup> parallelepipeds. The contacts were made by soldering with a

lead–tin solder. Their linearity was controlled using  $I$ – $V$  characteristics. The samples for measuring magnetization were cylinders of diameter  $d = 1$  mm and height  $h = 3$  mm. Magnetization  $M$  was measured in an ac magnetic field at a frequency  $\omega = 700$  Hz and atmospheric pressure. The induction method [8] was used to measure the isothermal magnetization under pressure in a zero magnetic field. The absolute accuracy of measuring the magnetization was 5%. A cylindrical sample (3.5–4 mm in length, 1.5 mm in diameter) was placed in two inductively coupled coils with at most  $n = 10$  turns. The magnetic field generated by the coils did not exceed 15 Oe.

The quality and the phase composition of the Zn<sub>0.1</sub>Cd<sub>0.9</sub>GeAs<sub>2</sub> + 10% MnAs and Zn<sub>0.1</sub>Cd<sub>0.9</sub>GeAs<sub>2</sub> + 15% MnAs samples were studied by X-ray diffraction (XRD), scanning electron microscopy (SEM), and energy dispersive spectroscopy (EDS). As follows from EDS analysis (spectrum 1) of the microsurface of a sample (inset to Fig. 1a), the samples had no any foreign elements (Fig. 1b). XRD data demonstrated that both compositions were characterized by the same positions of diffraction peaks, which corresponded to the presence of three crystalline phases in various ratios (Fig. 1a). The main phase was chalcopyrite Zn<sub>0.1</sub>Cd<sub>0.9</sub>GeAs<sub>2</sub> ( $I42d$ ) with lattice parameters  $a = 5.927$  Å and  $c = 11.212$  Å, and the two additional phases were cubic ZnGeAs<sub>2</sub> ( $F43m$ ) with  $a = 5.74$  Å and hexagonal MnAs ( $P63/mmc$ ) with  $a = 3.716$  Å and  $c = 5.748$  Å. The content of the impurity cubic phase was 16%. It should be noted that this phase forms naturally during the formation of the matrix material, namely, chalcopyrite Zn<sub>0.1</sub>Cd<sub>0.9</sub>GeAs<sub>2</sub>. Hexagonal MnAs clusters were randomly distributed in the semiconductor matrix. According to SEM, the average MnAs cluster sizes did not exceed 200 nm.

## 3. RESULTS AND DISCUSSION

The temperature dependences of magnetization  $M(T)$  were measured in a magnetic field  $H = 100$  Oe in the temperature range 270–350 K (see Fig. 2). The  $M(T)$  dependence points to ferromagnetic phase transitions at 310 and 312 K. Curie temperature  $T_C$  was determined from the inflection point in the  $M(T)$  curve, where the condition  $\partial^2 M / \partial T^2 \rightarrow 0$  is met. The determined values of  $T_C$  are given in Table 1, and they are seen to weakly change with the number of Mn ions in the material. Nevertheless,  $T_C$  can increase slightly in samples with a low or high Mn content because of deformation of MnAs clusters. For example, the authors of [15, 16] concluded that  $T_C$  changes mainly due to a change in the magnetic properties of MnAs clusters.

Magnetic susceptibility  $\chi = (\partial M / \partial H)_{\partial T = \text{const}}$  can be calculated using magnetization data determined at a constant temperature. The temperature dependence of inverse susceptibility at above  $T_C$ , i.e., in the para-

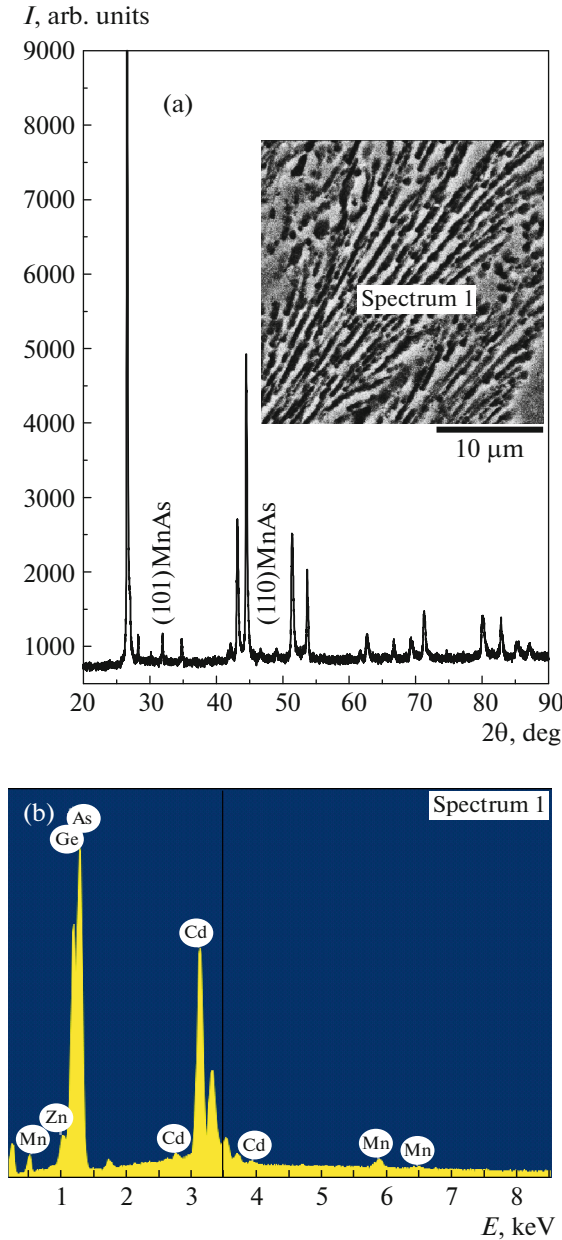


**Fig. 1.** (Color online) (a) X-ray diffraction pattern of the  $\text{Zn}_{0.1}\text{Cd}_{0.9}\text{GeAs}_2 + 10\% \text{MnAs}$  sample with the peaks corresponding to the hexagonal MnAs phase. (inset) SEM image of the  $\text{Zn}_{0.1}\text{Cd}_{0.9}\text{GeAs}_2 + 15\% \text{MnAs}$  sample, from the surface of which EDS spectra were taken. (b) Elemental composition of the sample.

magnetic region, should obey the Curie–Weiss law (Fig. 2),

$$\chi = \frac{C}{T - \Theta} + \chi_{\text{dia}}, \quad (1)$$

where  $C = N_0 g^2 \mu_B^2 S(S + 1) y_m / 3k_B$  is the Curie constant,  $\chi_{\text{dia}}$  is the diamagnetic contribution of the magnetic susceptibility of the lattice,  $N_0$  is the number of ions per gram,  $g$  is the  $g$  factor of the magnetic ion ( $g =$

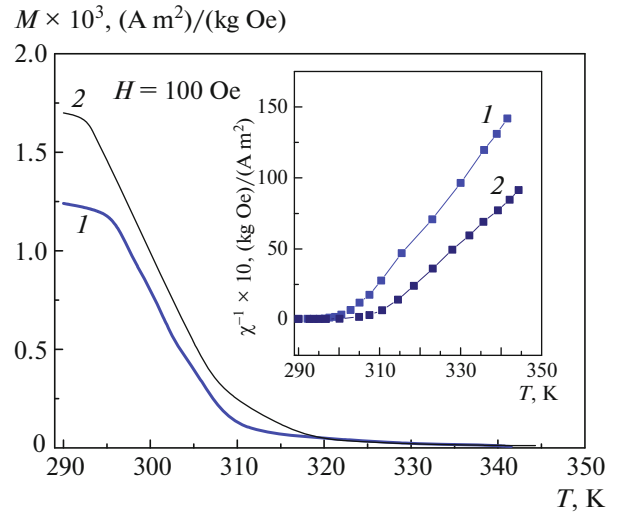


**Fig. 2.** (Color online) Calculated temperature dependences of the magnetization of (1)  $\text{Zn}_{0.1}\text{Cd}_{0.9}\text{GeAs}_2 + 10\% \text{MnAs}$  and (2)  $\text{Zn}_{0.1}\text{Cd}_{0.9}\text{GeAs}_2 + 15\% \text{MnAs}$ . (inset) Experimental temperature dependences of inverse magnetic susceptibility  $\chi^{-1}$  for these compositions.

2 for Mn),  $S = 5/2$  is the spin-magnetic moment of the Mn ion,  $\mu_B$  is the Bohr magneton,  $k_B$  is the Boltzmann constant, and  $y_m$  is the number of magnetically active Mn ions. Using the experimental data obtained in the temperature range  $T = 270\text{--}350$  K and Eq. (1), we calculated  $\chi(T)$  on the assumption that the diamagnetic contribution to the magnetic susceptibility remains constant. For the estimation, we used the value  $\chi_{\text{dia}} = -2 \times 10^{-4} (\text{A m}^2)/(\text{kg Oe})$  [17]. Using the experimental curve, we determined Curie–Weiss temperature  $\Theta$  and Curie constant  $C$ .

Figure 2 shows the calculated curves along with the experimental data. As is seen in the inset to Fig. 2, the magnetic susceptibilities of the samples are well described by the Curie–Weiss law.

The obtained values of  $C$  can be used to calculate the sum of magnetically active Mn ions by Eq. (1). Table 1 gives all parameters calculated for the samples under study. It should be noted that calculated  $y_m$  is lower than the total Mn content in the samples  $y$  [18]. This difference can be caused by the following factors: first, the Curie–Weiss law is valid for the range  $T > T_C$ , where Mn ions are not arranged along a field direction and their contributions to the magnetic susceptibility are partial; second, most Mn ions in the material are magnetically active or in the charge state  $\text{Mn}^{2+}$ , which differs from the high-spin state with a total magnetic moment  $J = S = 5/2$ . Moreover, as follows from Table 1, the closeness of  $\Theta$  and  $T_C$  indicates the absence of strong magnetic heterogeneities in the samples.

**Table 1.** Magnetic and transport properties of the samples at atmospheric pressure

Samples	$T_C$ , K	$C \times 10^{-1}$ , (A m <sup>2</sup> K)/kg	$\Theta$ , K	$R_H$ , cm <sup>3</sup> /C	$\rho$ , $\Omega$ cm	$y_m$	$y$ [16]
Zn <sub>0.1</sub> Cd <sub>0.9</sub> GeAs <sub>2</sub> + 10% MnAs	310	3.5	308	4.73	2.98	0.065	0.1
Zn <sub>0.1</sub> Cd <sub>0.9</sub> GeAs <sub>2</sub> + 15% MnAs	312	7.0	310	4.3	2.5	0.014	0.042

The results obtained can be explained as follows. The Zn<sub>0.1</sub>Cd<sub>0.9</sub>GeAs<sub>2</sub> + 10% MnAs and Zn<sub>0.1</sub>Cd<sub>0.9</sub>GeAs<sub>2</sub> + 15% MnAs composites are characterized by the presence of chaotically distributed Mn ions, the magnetic moments of which strongly interact with the magnetic moments of the hole subsystem (in the case of  $p$ -type materials), in a semiconductor matrix. The high magnetic exchange constants that are inherent in such magnetic semiconductors are caused by the chemical bond of the  $p$  and  $d$  orbitals [19].

Figure 3 shows the isothermal magnetization measured under pressure at  $T = 297$  K. As follows from this  $M(P)$  dependence,  $M$  decreases sharply at  $P > 3.2$  GPa, which results from a pressure-induced ferromagnet–paramagnet phase transition As was discussed in [8, 20], this sharp decrease in  $M$  can be

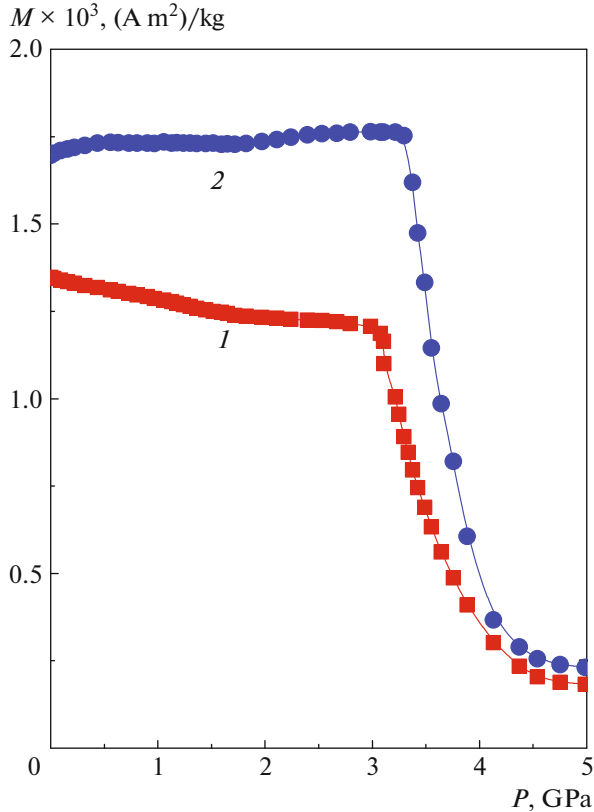


**Fig. 3.** (Color online) Magnetization vs. pressure for (1) Zn<sub>0.1</sub>Cd<sub>0.9</sub>GeAs<sub>2</sub> + 10% MnAs and (2) Zn<sub>0.1</sub>Cd<sub>0.9</sub>GeAs<sub>2</sub> + 15% MnAs at  $T = 297$  K.

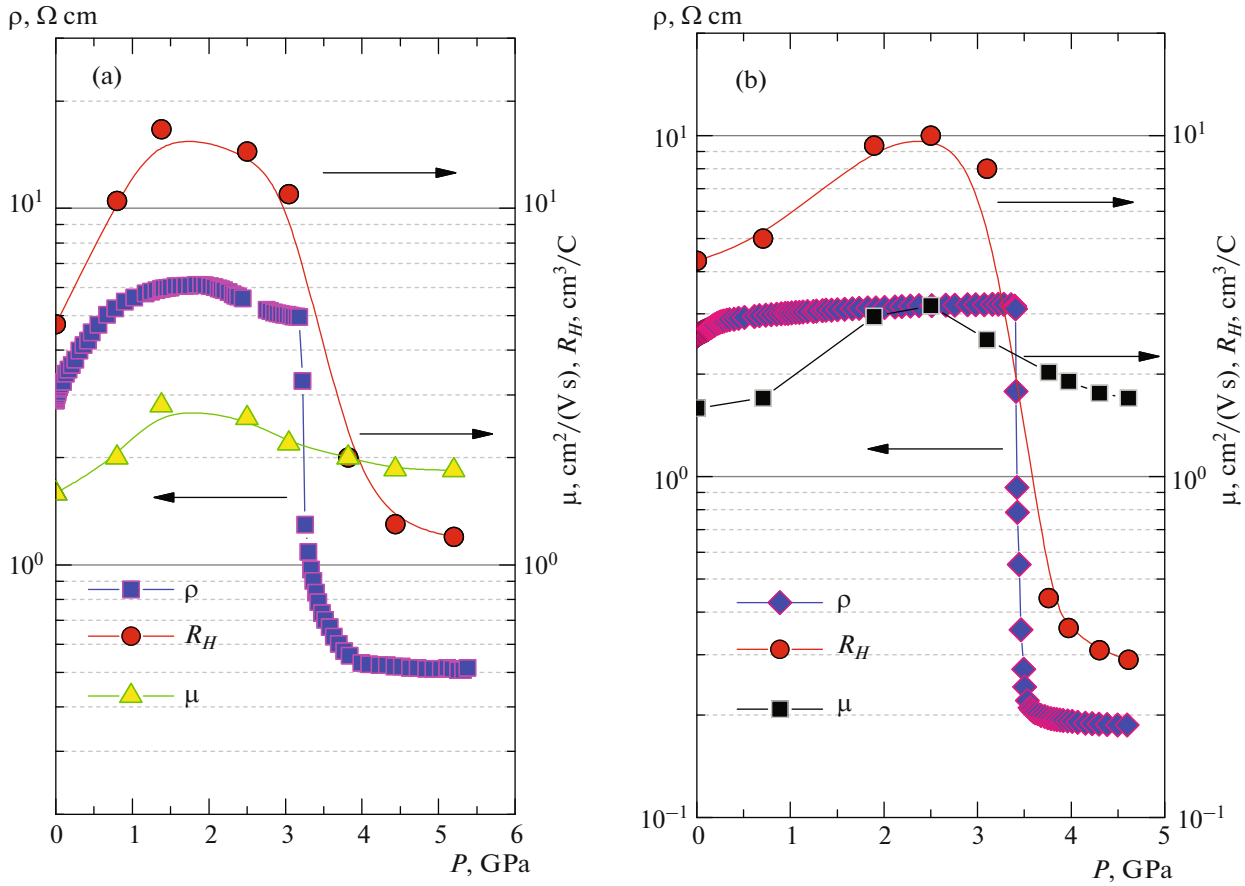
caused by a structural instability of the semiconductor matrix, i.e., a structural transition.

Along with the pressure-induced magnetic transition, the transport characteristics have a specific feature at a high pressure  $P > 3.2$  Ga. Figure 4 depicts the room-temperature baric dependences of electrical resistivity  $\rho(P)$ , Hall coefficient  $R_H(P)$  measured in a field of 5 kOe, and Hall mobility  $\mu_H(P)$  for Zn<sub>0.1</sub>Cd<sub>0.9</sub>GeAs<sub>2</sub> + 10% MnAs and Zn<sub>0.1</sub>Cd<sub>0.9</sub>GeAs<sub>2</sub> + 15% MnAs. The electrical resistivities of both samples increase and reach maxima at  $P \approx 2$  GPa and then decrease sharply (by more than an order of magnitude) at  $P > 3.5$  GPa. The Hall coefficient increases to  $P \approx 2$  GPa and then decreases sharply (by almost an order of magnitude) at  $P > 3.5$  GPa. In the saturation range at  $P > 5$  GPa, the transport parameters are as follows:  $\rho(P) \approx 0.5 \Omega$  cm and  $\mu_H(P) \approx 2.3$  cm<sup>2</sup>/(V s) for Zn<sub>0.1</sub>Cd<sub>0.9</sub>GeAs<sub>2</sub> + 10% MnAs and  $\rho(P) \approx 0.18 \Omega$  cm and  $\mu_H(P) \approx 1.7$  cm<sup>2</sup>/(V s) for Zn<sub>0.1</sub>Cd<sub>0.9</sub>GeAs<sub>2</sub> + 15% MnAs.

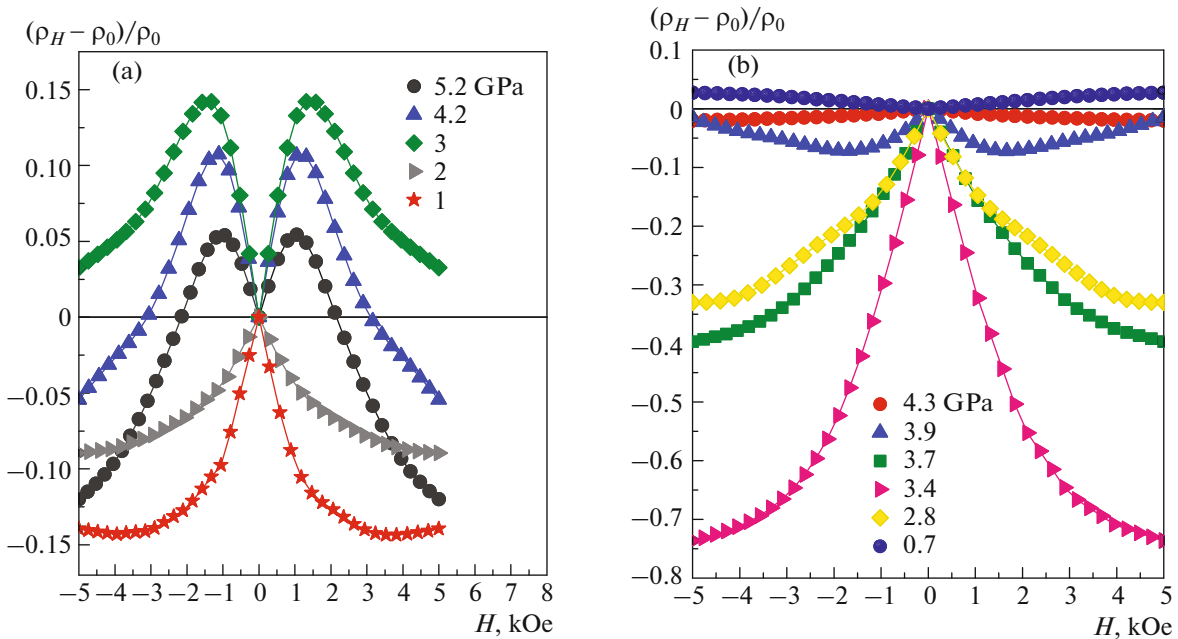
As follows from these significant changes in the  $\rho(P)$  and  $R_H(P)$  dependences (specifically, carrier concentration  $p = 1/eR_H$ , where  $R_H$  is an effective quantity), a semiconductor–metal transition takes place in the samples. The field dependence of the Hall resistance is linear in magnetic fields up to 5 kOe, which points to the absence of a contribution of the anomalous Hall effect and to the correctness of determining the carrier concentration. It should be noted that the noticeable change in the electron transport is caused by a structural transition, which is characteristic of chalcopyrite compounds [21].

Figure 5 shows the field dependences of MR, which is calculated as  $\Delta\rho/\rho_0 = (\rho_H - \rho_0)/\rho_0$  ( $\rho_0$  is the zero-field electrical resistivity) for Zn<sub>0.1</sub>Cd<sub>0.9</sub>GeAs<sub>2</sub> + 10% MnAs and Zn<sub>0.1</sub>Cd<sub>0.9</sub>GeAs<sub>2</sub> + 15% MnAs. Both samples exhibit an increase in the negative MR with the applied pressure in comparison with the initial values at atmospheric pressure ( $\Delta\rho_{xx}/\rho_0 < 1\%$ ). The composition with 10% MnAs exhibits a weak positive contribution at  $P = 1$  GPa and  $H > 3.5$  kOe, and the composition with 15% MnAs exhibits a weak positive MR at  $P = 0.7$  GPa.

The behavior of MR in the semiconductor–metal transition range in both compositions is intersecting. As follows from the baric dependences of MR, the application of pressure or an increase in the magnetic field induces both positive and negative MR in the



**Fig. 4.** (Color online) Pressure dependences of the transport properties measured at room temperature, namely, electrical resistivity  $\rho$ , Hall coefficient  $R_H$  measured in a field of 5 kOe, and Hall mobility  $\mu_H$  for (a)  $\text{Zn}_{0.1}\text{Cd}_{0.9}\text{GeAs}_2 + 10\% \text{ MnAs}$  and (b)  $\text{Zn}_{0.1}\text{Cd}_{0.9}\text{GeAs}_2 + 15\% \text{ MnAs}$ .



**Fig. 5.** (Color online) MR vs. magnetic field  $H$  for (a)  $\text{Zn}_{0.1}\text{Cd}_{0.9}\text{GeAs}_2 + 10\% \text{ MnAs}$  and (b)  $\text{Zn}_{0.1}\text{Cd}_{0.9}\text{GeAs}_2 + 15\% \text{ MnAs}$  at various pressures  $P$  and  $T = 297 \text{ K}$ .

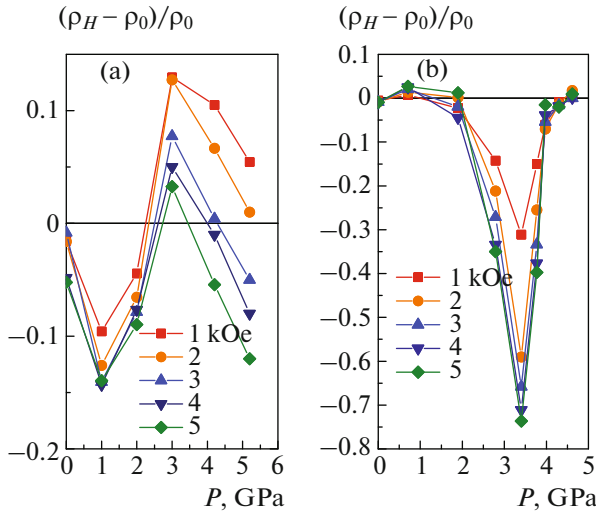


**Fig. 6.** (Color online) MR vs. pressure  $P$  for (a)  $\text{Zn}_{0.1}\text{Cd}_{0.9}\text{GeAs}_2 + 10\%$  MnAs and (b)  $\text{Zn}_{0.1}\text{Cd}_{0.9}\text{GeAs}_2 + 15\%$  MnAs in various magnetic fields  $H$  and  $T = 297$  K.

semiconductor–metal transition range at  $P > 3.5$  GPa (Fig. 6). The behavior of MR in the semiconductor–metal transition range in  $\text{Zn}_{0.1}\text{Cd}_{0.9}\text{GeAs}_2 + 10\%$  MnAs differs from the behavior of MR in  $\text{Zn}_{0.1}\text{Cd}_{0.9}\text{GeAs}_2 + 15\%$  MnAs. It should be noted that the MR of  $\text{Zn}_{0.1}\text{Cd}_{0.9}\text{GeAs}_2 + 15\%$  MnAs is negative and increases significantly to a maximum of about 74% in the semiconductor–metal transition range at  $P > 3.5$  GPa (Fig. 5). This transition in both compounds is accompanied by metallization with a carrier concentration  $p = 5.2 \times 10^{18}$  and  $2.0 \times 10^{19} \text{ cm}^{-3}$ , respectively (Fig. 4).

The presence of a magnetic Mn impurity implies that scattering at room temperature is mainly related to spin-dependent transport, since possible contributions, such as weak localization or microscopic conduction fluctuations, are predominant at low temperatures [22].

Thus, the detected negative and positive MRs can be considered in terms of a model based on the semiempirical Khosla–Fischer law [23],

$$\frac{\rho_H - \rho_0}{\rho_0} = -a^2 \ln(1 + b^2 H^2) + \frac{c^2 H^2}{1 + d^2 H^2}. \quad (2)$$

Here, fundamental parameters  $a$  and  $b$  are related to the nature of exchange interaction, and parameters  $c$  and  $d$  describe the two-band transport in a spin-split valence band [6]. Nevertheless, the application of this expression seems to be restricted, since the nature of magnetic scattering can be caused by both the localized moments of Mn in the substituted structure of the semiconductor and the presence of MnAs clusters. An analysis of the negative MR of  $\text{Zn}_{0.1}\text{Cd}_{0.9}\text{GeAs}_2 + 15\%$

MnAs with Eq. (2) implies that the scattering mechanisms in the semiconductor–metal transition range belong to the nature of the  $p$ – $d$  interaction that appears between current carriers (holes) and the magnetic moment localized at an Mn impurity [24].

The situation at low pressures is thought to be complex. In particular, the positive MR at  $P \approx 0.7$  GPa cannot be correctly described with the right-hand side of Eq. (2), since the MR in weak magnetic fields obeys a linear law instead of the proposed behavior, which is proportional to  $H^2$ . Thus, we can speak about the presence of other contributions, which are predominant far from the semiconductor–metal transition range, to the resulting effect. It should be noted that the predominant positive MR is likely not to be caused by the pure  $p$ – $d$  hybridization of the valence band [6, 23]: it is thought to be supplemented with enhancement of the electron–electron interaction [3], which is most likely to occur during the structural transformation.

The appearance of colossal MR in the vicinity of the semiconductor–metal transition [25] was attributed to the appearance of magnetic polarons, which form in the  $\text{EuB}_6$  matrix during the transition into a ferromagnetic phase [26, 27]. Our experimental results do not give obvious signs of a polaron mechanism in  $\text{Zn}_{0.1}\text{Cd}_{0.9}\text{GeAs}_2 + \text{MnAs}$ . The enhancement of negative MR detected in this work is closely related to the structural transformation, which induce changes in the electron transport and the magnetic state of MnAs clusters. Similar pressure-induced negative MR was observed in a number of semiconductors doped with magnetic impurities (in particular, Mn). For example,  $\text{CdGeAs}_2 : \text{Mn}$  and  $\text{CdGeP}_2 : \text{Mn}$  samples exhibited positive (at  $P < 2$  GPa) and negative ( $P > 2$  GPa) MR, which was about 0.7% in  $\text{CdGeP}_2 : \text{Mn}$  and 1.5% in  $\text{CdGeAs}_2 : \text{Mn}$ , respectively, in the pressure range up to 5 GPa and magnetic fields  $H \leq 5$  kOe [28–30].

#### 4. CONCLUSIONS

The sign of MR in  $\text{Zn}_{0.1}\text{Cd}_{0.9}\text{GeAs}_2 + 10\%$  MnAs and  $\text{Zn}_{0.1}\text{Cd}_{0.9}\text{GeAs}_2 + 15\%$  MnAs, which have Curie temperatures  $T_C \approx 310$ – $312$  K, changed, and the negative contribution to MR was found to be predominant over a wide pressure range. This behavior results from pressure-induced magnetic and structural transitions and a semiconductor–metal transition, which significantly enhance MR in the range of these phase transitions. In particular, a magnetic ferromagnet–paramagnet transition is only attributed to MnAs clusters at  $P > 3.2$  GPa, which is caused by a structural change in the matrix. In this pressure range, the mechanisms that are responsible for enhanced MR are assumed to have a spin-dependent character of scattering by magnetic Mn impurities in the matrix of the  $\text{Zn}_{0.1}\text{Cd}_{0.9}\text{GeAs}_2$  semiconductor.

## FUNDING

This work was supported by the Ministry of Education and Science of the Russian Federation (State assignment no. 0203-2019-0008). One of the authors (T.R.A) is grateful to the Russian Foundation for Basic Research (project no. 19-02-00031). The samples were synthesized by I.V.F. and A.L.Zh. and the synthesis was supported by the Russian Foundation for Basic Research, project no. 17-53-04055 Bel\_mol\_a.

## REFERENCES

- H. Akinaga, *Semicond. Sci. Technol.* **17**, 322 (2002).
- D. D. Dung and S. Cho, *J. Appl. Phys.* **113**, 17C734 (2013).
- D. V. Baxter, R. Richter, M. L. Trudeau, R. W. Cochrane, and J. O. Strom-Olsen, *J. de Phys.* **50**, 1673 (1989).
- L. P. Rokhinson and Y. Lyanda-Geller, Z. Ge, S. Shen, X. Liu, M. Dobrowolska, and J. K. Furdyna, *Phys. Rev. B* **76**, 161201(R) (2007).
- C. Haas, *Phys. Rev.* **168**, 531 (1968).
- J. A. Peters, N. D. Parashar, N. Rangaraju, and B. W. Wessels, *Phys. Rev. B* **82**, 205207 (2010).
- M. Csontos, T. Wojtowicz, X. Liu, M. Dobrowolska, B. Janko[acute], J. K. Furdyna, and G. Mihály, *Phys. Rev. Lett.* **95**, 227203 (2005).
- T. R. Arslanov, L. Kilanski, S. López-Moreno, A. Yu. Mollaev, R. K. Arslanov, I. V. Fedorchenko, T. Chatterji, S. F. Marenkin, and R. M. Emirov, *J. Phys. D* **49**, 125007 (2016).
- R. G. Dzhamedov, T. R. Arslanov, A. Yu. Mollaev, and A. V. Kochura, *J. Alloys Compd.* **699**, 1104 (2017).
- Y. D. Park, A. Wilson, A. T. Hanbicki, J. E. Mattson, T. Ambrose, G. Spanos, and B. T. Jonker, *Appl. Phys. Lett.* **78**, 2739 (2001).
- K. Suenaga, S. Higashihara, M. Ohashi, G. Oomi, M. Hedo, Y. Uwatoko, K. Saito, S. Mitani, and K. Takahashi, *Phys. Rev. Lett.* **98**, 207202 (2007).
- M. Csontos, G. Mihály, B. Jankó, T. Wojtowicz, X. Liu, and J. K. Furdyna, *Nat. Mater.* **4**, 447 (2005).
- L. G. Khvostantsev, V. N. Slesarev, and V. V. Brazhkin, *High Press. Res.* **24**, 371 (2004).
- I. V. Fedorchenko, A. N. Aronov, L. Kilanski, V. Domukhovski, A. Reszka, B. J. Kowalski, E. Lähderanta, W. Dobrowolski, A. D. Izotov, and F. Marenkin, *J. Alloys Compd.* **599**, 121 (2014).
- J. H. Song, Y. Cui, and J. B. Ketterson, *J. Appl. Phys.* **111**, 07E125 (2012).
- M. Bolzan, I. Bergenti, G. Rossetto, P. Zanella, V. Dediu, and M. Natali, *J. Magn. Magn. Mater.* **316**, 221 (2007).
- L. Kilanski, K. Szałowski, R. Szymczak, M. Górka, E. Dynowska, P. Aleshkevych, A. Podgórn, A. Avdonin, W. Dobrowolski, I. V. Fedorchenko, and S. F. Marenkin, *J. Appl. Phys.* **114**, 093908 (2013).
- L. Kilanski, I. V. Fedorchenko, M. Górka, A. Ślowska-Waniewska, N. Nedelko, A. Podgórn, A. Avdonin, E. Lähderanta, W. Dobrowolski, A. N. Aronov, and S. F. Marenkin, *J. Appl. Phys.* **118**, 103906 (2015).
- P. M. Krstajić, F. M. Peeters, V. A. Ivanov, V. Fleurov, and K. Kikoin, *Phys. Rev. B* **70**, 195215 (2004).
- T. R. Arslanov, A. Yu. Mollaev, I. K. Kamilov, R. K. Arslanov, L. Kilanski, R. Minikaev, A. Reszka, S. López-Moreno, A. H. Romero, M. Ramzan, P. Panigrahi, R. Ahuja, V. M. Trukhan, T. Chatterji, S. F. Marenkin, and T. V. Shoukavaya, *Sci. Rep.* **5**, 7720 (2015).
- A. Yu. Mollaev, R. K. Arslanov, I. K. Kamilov, T. R. Arslanov, U. Z. Zalibekov, and I. V. Fedorchenko, *Russ. J. Inorg. Chem.* **60**, 994 (2015).
- I. V. Fedorchenko, L. Kilanski, I. Zakharchuk, P. Geydt, E. Lähderanta, P. N. Vasilyev, N. P. Simonenko, A. N. Aronov, W. Dobrowolski, and S. F. Marenkin, *J. Alloys Compd.* **650**, 277 (2015).
- B. P. Khosla and J. B. Fischer, *Phys. Rev.* **6**, 4073 (1972).
- T. R. Arslanov, R. K. Arslanov, I. V. Fedorchenko, L. Kilanski, and T. Chatterji, *JETP Lett.* **107**, 612 (2018).
- S. Söllow, I. Prasad, M. C. Aronson, J. L. Sarrao, Z. Fisk, D. Hristova, A. H. Lacerda, M. F. Hundley, A. Vigliante, and D. Gibbs, *Phys. Rev. B* **57**, 5860 (1998).
- P. Nyhus, S. Yoon, M. Kauffman, S. L. Cooper, Z. Fisk, and J. Sarrao, *Phys. Rev. B* **56**, 2717 (1997).
- L. Degiorgi, E. Felder, H. R. Ott, J. L. Sarrao, and Z. Fisk, *Phys. Rev. Lett.* **79**, 5134 (1997).
- A. Yu. Mollaev, I. K. Kamilov, R. K. Arslanov, T. R. Arslanov, U. Z. Zalibekov, V. M. Novotortsev, and S. F. Marenkin, *JETP Lett.* **91**, 478 (2010).
- A. Yu. Mollaev, I. K. Kamilov, R. K. Arslanov, T. R. Arslanov, U. Z. Zalibekov, V. M. Novotortsev, S. F. Marenkin, and V. M. Trukhan, *Appl. Phys. Lett.* **100**, 202403 (2012).
- T. R. Arslanov, A. Yu. Mollaev, I. K. Kamilov, R. K. Arslanov, U. Z. Zalibekov, V. V. Mamedov, S. F. Marenkin, S. A. Varnavsky, and V. M. Trukhan, *Int. Rev. Phys.* **6**, 4 (2012).

*Translated by K. Shakhlevich*